AIMS Mathematics, 8(1): 164–193.
DOI: 10.3934/math.2023008
Received: 24 July 2022
Revised: 28 August 2022
Accepted: 15 September 2022
Published: 27 September 2022

http://www.aimspress.com/journal/Math

Research article

Heat transport and magnetohydrodynamic hybrid micropolar ferrofluid flow over a non-linearly stretching sheet

Abdul Rauf[1,†], Nehad Ali Shah[2,†], Aqsa Mushtaq[1] and Thongchai Botmart[3,*]

[1] Department of Mathematics, Air University Multan Campus, Chak 5-Faiz, Bahawalpur Road, Multan, Pakistan
[2] Department of Mechanical Engineering, Sejong University, Seoul 05006, South Korea
[3] Department of Mathematics, Faculty of Science, Khon Kaen University, Khon Kaen, 40002, Thailand

* **Correspondence:** Email: thongbo@kku.ac.th.

† These authors contributed equally to this work and are co-first authors.

Abstract: A stable colloid called ferrofluid is made up of tiny magnetic particles, often magnetite (Fe_3O_4), that have been bonded with an amphiphilic dispersion layer and are then suspended in a suitable liquid solvent carrier. Current industrial uses for ferrofluid include dynamic sealing, inertial and viscous damping, magnetic drug targeting, liquid microrobots, etc. In this article, we studied the heat transfer and MHD micropolar ferrofluid flow caused by non-linearly stretching surface. The results are presented for hybrid alumina- copper/ethylene glycol (Al_2O_3-Cu/EG) nanofluid. The governing non-linear equations describing flow are transformed into a system of ordinary differential equations using similarity transformations. Using the BVp4c method, the microstructure and inertial properties of a magnetite ferrofluid across a non-linear stretched sheet are studied. The influence of relevant parameters on stream function, velocity, micro-rotation velocity, and temperature are obtained and represented graphically. The computed results are original, and it has been observed that if we increase the magnetic parameter, the stream function and the velocity decrease, while the temperature and micro-rotation velocity increase. As the Prandtl number increases, the temperature profile decreases. It has been observed that the Nusselt number or heat transfer rate of hybrid nanofluid is better as compared to nanofluid flow.

Keywords: ferrofluid; nonlinearly stretching sheet; MHD flow; hybrid nanofluid; ferrohydrodynamic

Mathematics Subject Classification: 76D05, 76A02, 65L10

1. Introduction

In order to meet industrial and technical requirements, a smart fluid with exceptional thermal capabilities is desired. A novel heat transfer fluid created using nanotechnology termed a nanofluid was first described by Choi [1] in 1955. A growing proportion of nanotechnology for heat transmission is called nanofluids, which are colloidal mixtures of nanoparticles (1–100 nm) and a base liquid (nanoparticle fluid suspensions) (see Buongiorno et al. [2]). Figure 1 shows a comparative sample of different sizes of materials from large scales to nanoscales. Polymers, metals, metal oxides, and other substances may all be found in nanofluids. The thermophysical properties of traditional thermal fluids are improved significantly by the inclusion of nanoparticles, improving the heat transfer coefficient. Nanofluids are currently widely used in a number of industries, including the electronics, automotive, solar energy, medicinal, and oil recovery industries, as a result of such a wider acceptance (see Singh et al. [3] and Suvardhan et al. [4]).

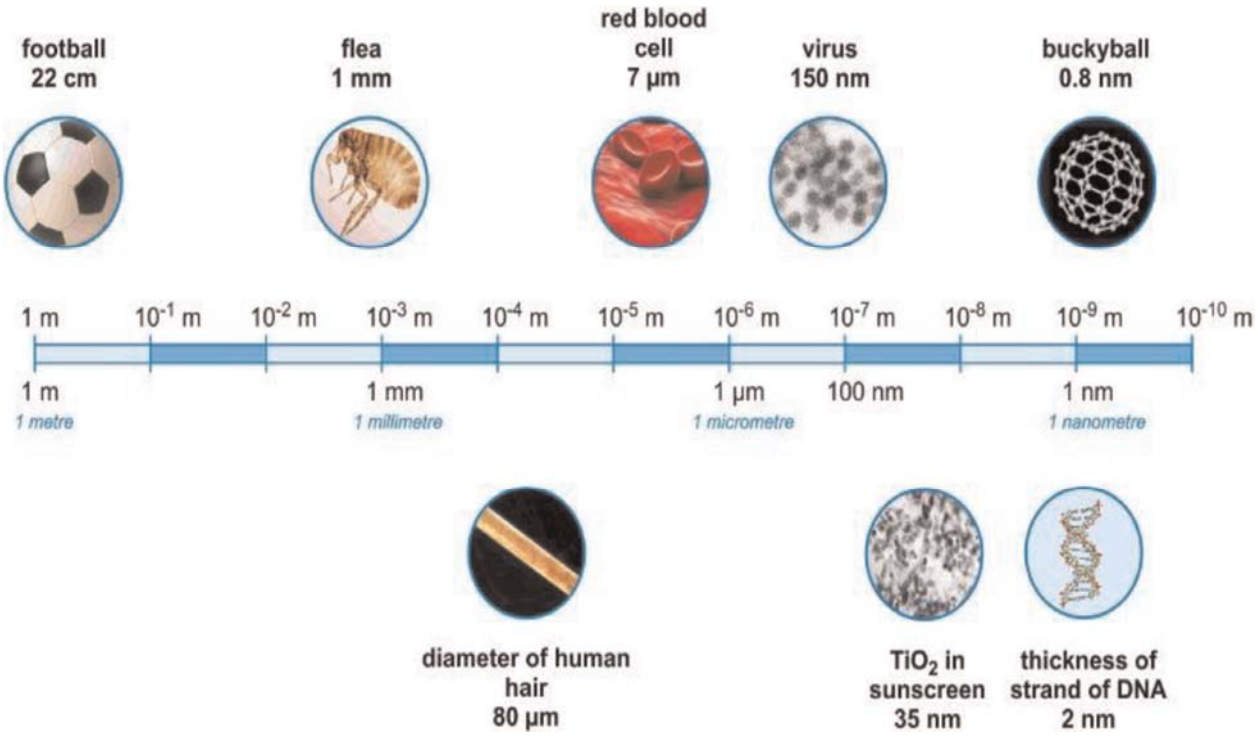

Figure 1. A comparative of things from large scale to nanoscale.

Researchers are presently drawn to hybrid and dihybrid nanofluid due to the advantages of nanofluid and the growing study into flow, heat, and mass transport phenomena. Hybrid nanofluid is the term used to describe a combination that contains several nanoparticles. It is referred to as a "dihybrid nanofluid" if the combination contains several nanoparticles and fluids [5]. According to Lou et al. [6], the key benefit of hybrid nanofluids is increased energy efficiency, conservation, and savings. In order to achieve uniform shear flow over a stretched sheet, Waini et al. [7] investigated the effects of transpiration on the hybrid nanofluid flow. They discovered that an improvement in copper

nanoparticle volume fractions results in an improvement in heat transmission.

The heat conduction study of a stretching surface constantly moving along an ambient fluid has received a lot of attention and has been widely described in the literature. The composition of the ambient liquid and the pace of stretching determines the properties of products created through engineering procedures such as metallurgy and polymer extrusion. Because quick stretching or irregular temperature changes in the extrudate can compromise the intended qualities of the last product, the heat exchange rate must be exactly controlled. Nanofluids are mixtures of a base fluid and nanoparticles that are homogeneous. The particles in these suspensions can be metal or non-metal. Ferrofluid is a class of nanofluid in which the suspension of nanoparticles can be magnetized. Ferrofluids offer a lot of potential in these kinds of applications. Ferrofluids are fluids made artificially from extremely reduced mixture suspensions of tiny magnetic molecules suspended in a carrier fluid that is not conducting. This fluid acts normally except for the fact that it is subjected to a force owing to magnetization. Ferrohydrodynamics is the study of magnetic fluid motion mechanics that is transformed by strong magnetic polarization forces. The existence of an external magnetic source may affect significantly the dynamics of electrically conducting fluids flowing effectively in its spawned field [8]. The effects of magnetization on fluid flow with magnets were first described by Rosensweig [9]. In the last several years, for Newtonian and non-Newtonian fluids, as well as flat horizontal surfaces, flow and heat transfer have been extensively studied under various hydrodynamic and thermal boundary conditions [10–12]. Near the infinite plate, heat transport and magnetohydrodynamic (MHD) flow have been investigated. To make a ferrofluid flow, Andersson and Valnes [13] were the first to use a stretched surface with a magnetic dipole. Andersson [13–14] showed that the impact of an externally provided magnetic field on flow is similar to that of viscoelasticity.

The effects of nonlinear stretching or shrinking on MHD flow are discussed [15–17]. For flow past a stretching/shrinking sheet, two solutions were discovered in [18]. Furthermore, it's crucial to research boundary layer flow and heat transmission across a stretched surface, because it has a wide range of uses in industrial engineering and production processes, such as plastic sheet aerodynamic expulsion and paper manufacturing, manufacture of glass fiber. In the polymer sector, heat-treated materials are transported between feed and wind-up rolls, drawing using wires, whirling metal, and many others [19–22]. Hayat et al. [23] also came up with a solution based on an analysis of a second-grade fluid's slip flow and heat transfer through a planar stretching sheet. Martin and Boyd [24] looked at the steady wall temperature, heat transfer, and slide flow past a flat surface. Their findings show that boundary layer equations may be utilized to examine flow at the microelectromechanical systems (MEMS) scale and that they can be used to investigate rarefaction's impact on shear stress and flow structure. In chemical industries, such as the development of nuclear waste disposal canisters and the cooling systems for nuclear reactors, it's common to employ mixed convectional flow with heat transmission. These physical processes take place when the effects of buoyant forces become even more powerful. Ali [25] looked into the impact of viscosity that varies with temperature on heat transmission via laminar mixed convection along a surface that is constantly shifting. According to the literature study, there are just a few research on heat transmission from ferrofluids. Li and Xuan [26] explored the effects of an external magnetic field on convective heat transport using a ferrofluid flow through a thin wire. They discovered that the magnetic field from the outside affects the ferrofluids' heat transmission via convection performance. When Yamaguchi et al. [27] analyzed the convection naturally of the fluid with magnetic properties in a square hollow with partitions having a magnetic field imposed from the outside computationally, they discovered that a substantial magnetic field

influences the convection flow. Motozawa et al. [28] explored the influence of heat transfer in a magnetic fluid flow with a magnetic field in a duct that is rectangular. They observed that the heat transfer coefficient rises locally in the presence of a magnetic field. The coefficient of heat transfer increases as the magnetic field increases. Characteristics of ferrofluid flow over a linearly stretching have already been discussed in previous work.

The thorough review of the literature demonstrates that, the study of heat transfer and MHD hybrid nano-fluid with micropolar ferrofluid flow over a non-linearly stretching sheet does not exist in literature. In this article, we considered this problem with two different nanoparticles (Al_2O_3-Cu) suspended in the base fluid ethylene glycol (EG). Using the suitable similarity transformations, the governing equations are transformed into a set of nonlinear ordinary differential equations, which are then solved using the built-in MATLAB module BVP-4c.

2. Materials and methods

The topic of micropolar and classical nanofluid across a stretched sheet has been studied by several researchers. The flow of a micropolar/classical ferrofluid on a stretched sheet in the y > 0 regions was presumed steady-state in this research. At x=0, the surface is stretched in the x-direction and normal in the y-direction. The stretched sheet's surface velocity is $u_w(x) = ax^m$, where a is an optional constant that is positive. A magnetic field perpendicular to the surface is also present (See Figure 2). Here are the micropolar ferrofluid governing equations based on the preceding assumptions:

The continuity equation and momentum equations are [29],

$$\frac{\mathrm{d}}{\mathrm{dt}}(\rho_{\mathrm{hnf}}\mathrm{V}) = \nabla\cdot(\rho_{\mathrm{hnf}}\mathrm{V}) \tag{1}$$

$$\rho_{hnf}\left(\frac{dV}{dt}\right) = -\nabla \mathrm{p} + \left(2\mu_{\substack{hn\\f}} + k\right)\nabla(\nabla\cdot V) - \left(\mu_{hnf} + k\right)\nabla\times(\nabla\times V) + k(\nabla\times N) + J\times B + \rho_{hnf} \tag{2}$$

$$\rho_{hnf} j\left(\frac{dN}{dt}\right) = \left(\varphi + \lambda + \gamma_{hnf}\right)\nabla\cdot\left(\rho_{hnf}\cdot N\right) - \gamma_{hnf}\nabla\times(\nabla\times N) + k(\nabla\times v) - 2kN + \rho_{hnf} I \tag{3}$$

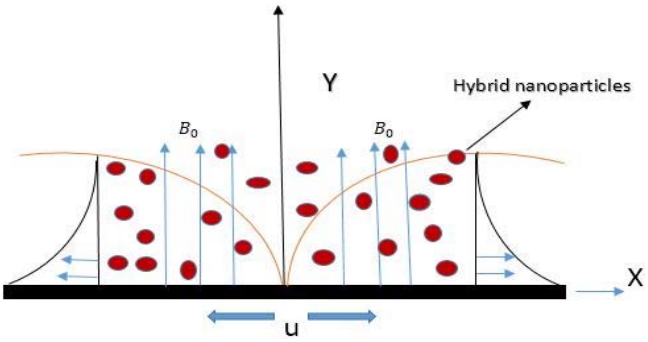

Figure 2. Flow Geometry.

The thermophysical properties $\mu_{hnf}(\beta)$, ρ_{hnf}, K_{hnf}, $(\rho\beta_T)_{hnf}$, $(\rho\beta_C)_{hnf}$, $(\rho C_p)_{hnf}$ and σ_{hnf} for hybrid nanofluid (Al_2O_3-Cu/EG) are defined as,

$$\rho_{hnf} = (1-\phi_2)\left[(1-\phi_1)\rho_f + \phi_1\rho_{s1}\right] + \phi_2\rho_{s2}, \tag{4}$$

$$(\rho C_P)_{hnf} = (1-\phi_2)\left[(1-\phi_1)(\rho C_P)_f + \phi_1(\rho C_P)_{s1}\right] + \phi_2(\rho C_P)_{s2}, \tag{5}$$

$$(\rho\beta_T)_{hnf} = (1-\phi_2)\left[(1-\phi_1)(\rho\beta_T)_f + \phi_1(\rho\beta_T)_{s1}\right] + \phi_2(\rho\beta_T)_{s2}, \tag{6}$$

$$(\rho\beta_C)_{hnf} = (1-\phi_2)\left[(1-\phi_1)(\rho\beta_C)_f + \phi_1(\rho\beta_C)_{s1}\right] + \phi_2(\rho\beta_C)_{s2}, \tag{7}$$

$$\frac{\mu_{hnf}}{\mu_f} = \frac{1}{(1-\phi_1)^{2.5}(1-\phi_2)^{2.5}}, \tag{8}$$

$$\frac{k_{hnf}}{k_{bf}} = \frac{k_{s2}+2k_{bf}-2\phi_2(k_{bf}-k_{s2})}{k_{s2}+2k_{bf}+\phi_2(k_{bf}-k_{s2})}, \tag{9}$$

where,

$$\frac{k_{bf}}{k_f} = \frac{k_{s1}+2k_f-2\phi_1(k_f-k_{s1})}{k_{s1}+2k_f+\phi_1(k_f-k_{s1})}, \tag{10}$$

$$\frac{\sigma_{hnf}}{\sigma_{bf}} = \frac{\sigma_{s2}+2\sigma_{bf}-2\phi_2(\sigma_{bf}-\sigma_{s2})}{\sigma_{s2}+2\sigma_{bf}+\phi_2(\sigma_{bf}-\sigma_{s2})}, \tag{11}$$

where,

$$\frac{\sigma_{bf}}{\sigma_f} = \frac{\sigma_{s1}+2\sigma_f-2\phi_1(\sigma_f-\sigma_{s1})}{\sigma_{s1}+2\sigma_f+\phi_1(\sigma_f-\sigma_{s1})}, \tag{12}$$

where ϕ_1, ϕ_2 are solid volume fraction of Alumina/Aluminium oxide, Cuprum/Copper, respectively, C_p is the specific heat, k_f denotes the thermal conductivity of the regular fluid. The values for the thermophysical parameters for hybrid nanofluid (Al_2O_3-Cu/EG) is shown in Table 1.

Table 1. Physical property parameters of the base fluid and nanoparticles.

Thermophysical property	Fluid (EG)	Alumina (Al_2O_3)	Cu
$\rho(kg/m^3)$	1114.0	3970	8933
$c_p(j/kg.K)$	2415	765	385
$k(w/m.K)$	0.2520	40	400
$\sigma(s/m)$	5.50×10^{-6}	59.6×10^{6}	35×10^{6}

Also, flow is incompressible with no external forces, and the governing equations are:

$$\rho_{hnf}\left(\frac{dv}{dt} + (v.\nabla)v\right) = \left(\mu_{hnf} + k\right)\nabla^2 v + k(\nabla\times N) + J\times B, \tag{13}$$

$$\rho_{hnf} j \left(\frac{dN}{dt} + (N.\nabla)N\right) = \gamma_{hnf}\nabla^2 N + k(\nabla \times v) - 2kN. \tag{14}$$

The body force proposed by Hussanan et al. is:

$$J \times B = -\sigma_{hnf} B_0^2 v. \tag{15}$$

The governing equations (momentum equations) take the form [30,31],

$$\rho_{hnf}\left(u\frac{\partial u}{\partial x} + v\frac{\partial u}{\partial y}\right) = \left(\mu_{hnf} + k\right)\frac{\partial^2 u}{\partial y^2} + k\frac{\partial N}{\partial y} - \sigma_{hnf} B_0^2 u, \tag{16}$$

$$\rho_{hnf} j \left(u\frac{\partial N}{\partial x} + v\frac{\partial N}{\partial y}\right) = \gamma_{hnf}\frac{\partial^2 N}{\partial y^2} - k(2N + \frac{\partial u}{\partial y}). \tag{17}$$

The energy equation is

$$u\frac{\partial T}{\partial x} + v\frac{\partial T}{\partial y} = \frac{k_{hnf}}{(c_p)_{nf}}\frac{\partial^2 T}{\partial y^2} - \frac{\partial q_r}{\partial y}\ , \tag{18}$$

and, according to Rosseland's guess, it is

$$u\frac{\partial T}{\partial x} + v\frac{\partial T}{\partial y} = \frac{1}{(c_p)_{hnf}}(k_{hnf} + \frac{16\sigma^* T_\infty^3}{3k^*})\frac{\partial^2 T}{\partial y^2}. \tag{19}$$

The problem's boundary conditions are

$$u = ax^m, \quad v = 0, \quad T = T_w, \quad N = -\delta\frac{\partial u}{\partial y}, \quad at\ y = 0, \tag{20}$$

$$u = 0, \quad T = T_\infty, \quad N = 0, \quad at\ y \to \infty. \tag{21}$$

For a better understanding of these formulas, the velocity components in the x and y directions are assumed to be u and v, respectively. The angular velocity is denoted by N. μ is viscosity in a dynamic state, δ is a constant in the $0 \le \delta \le 1$ region. When $\delta = 0$, microelements close to the wall surface are not allowed to spin. If $\delta = \frac{1}{2}$ demonstrated the insufficiency for the concentration of microelements. Furthermore, $\delta = 1$ when δ involve in the turbulent boundary layer flow. Micro inertia per unit mass is j, γ is the viscosity of a spinning gradient and k is the viscosity of the vortex. To solve these nonlinear differential equations quickly and easily, we made use of similarity transformations such as,

$$u = ax^m f',\ v = -\sqrt{\frac{2\nu a x^{m-1}}{(m+1)}}(\frac{(m+1)}{2}f + \frac{(m-1)}{2}\eta f'),\ \eta = \sqrt{\frac{(m+1)ax^{m-1}}{2\nu}}y,\ \theta(\eta) = \frac{(T-T_\infty)}{(T_w-T_\infty)},$$

$$N = a^{\frac{3}{2}}x^{\frac{(3m-1)}{2}}\sqrt{\frac{(m+1)}{2}}G. \tag{22}$$

By replacing the variables into the Eqs (16), (17), (19)–(21), we have

$$(e_2 + K)\frac{(m+1)}{2}f''' + e_1\frac{(m+1)}{2}ff'' - e_1 m f'^2 + KG'\frac{(m+1)}{2} - M^2 e_3 f' = 0, \tag{23}$$

$$\left(e_2+\frac{K}{2}\right)\frac{(m+1)}{2}G''+e_1\left(\frac{(m+1)}{2}fG'-\frac{(3m-1)}{2}f'G\right)-K_l(2G+f'')=0, \tag{24}$$

$$\frac{1}{e_5.P_r}(e_4+R)\theta''+\theta' f=0. \tag{25}$$

And the boundary conditions are

$$f'=1, f=0, \theta(\eta)=1, f''=-{}^{G}/_{\delta}\ at\ \eta=0, \tag{26}$$

$$f'\to 0, \theta(\eta)\to 0, G\to 0\ at\ \eta\to\infty. \tag{27}$$

The non-dimensional variables are subsequently presented

$$M^2=\frac{\sigma_f B_0^2}{a\rho_f}x^{1-m}, K=\frac{k}{\mu_f}, K_l=\frac{k}{\mu_f}x^{1-m}, j=\frac{\nu_f}{\alpha},\ Pr=\frac{(\rho c_p)_f \upsilon_f}{k_f}, R=\frac{16\sigma^* T_\infty^3}{3k^*\cdot k_f}, \tag{28}$$

and,

$$e_1=\frac{\rho_{hnf}}{\rho_f}, e_2=\frac{\mu_{hnf}}{\mu_f}, e_3=\frac{\sigma_{hnf}}{\sigma_f}, e_4=\frac{k_{hnf}}{k_f}\ \text{and}\ e_5=\frac{(\rho cp)_{hnf}}{(\rho cp)_f}, \tag{29}$$

where K represents the Micro-rotation parameter, K_l is the local micro-rotation parameter, j is micro-inertia density, R is radiative parameter stretching and Pr is Prandtl number.

3. Engineering quantities of interest

For this modeled flow problem, the skin friction coefficient and Nusselt, Sherwood number are defined as

$$C_f=\tau_z/\rho_f, Nu=\frac{q_w}{k_f(T_w-T_\infty)}, Sh=xq_m/D_B, \tag{30}$$

where q_w represents surface heat flux, τ_z denotes surface shear stress, and q_m defines surface mass flux for ferrofluid:

$$\tau_z=[\mu_{hnf}(\frac{\partial u}{\partial y})]_{y=0}, \quad q_w=-K[\frac{\partial T}{\partial y}]_{y=0}, q_m=-D_B[\frac{\partial N}{\partial Y}]_{y=0}. \tag{31}$$

Now apply the similarity transformation Eq (22) to both Eqs (30) and (31), and we get the results:

$$C_f(Re_x)^{-({}^1/_2)}=f''(0), \mathrm{N}u_x(Re_x)^{-({}^1/_2)}=-\theta'(0),\ Sh_x(Re_x)^{-({}^1/_2)}=-G'(0). \tag{32}$$

4. Numerical results and discussion

In this article, a numerical approach is used to investigate and assess some of the physical parameters of the ferrofluid flow over a stretching sheet, such as stream function $f(\eta)$, velocity $f'(\eta)$,

micro-rotation velocity $G(\eta)$, and temperature $\theta(\eta)$. The numerical solution of nonlinear coupled differential equations is obtained by using the MATLAB software BVP4c method. Figures 3 and 4 depict that with the increase in the weakness of concentration of microelement δ, the stream function $f(\eta)$ and the velocity $f'(\eta)$ decreases. Whereas the effect of the weakness of concentration of micro-element δ on the micro-rotating velocity $G(\eta)$ and temperature $\theta(\eta)$ is opposite as can be seen from Figures 5 and 6. Figures 7, 8, and 10 exhibit that with the increase in micro-rotation parameter K, the stream function $f(\eta)$ and velocity $f'(\eta)$ and micro-rotation velocity $G(\eta)$ increase. While the effect of micro-rotation parameter K on temperature is converse as is visible in Figure 9. Figure 11 shows that the stream function $f(\eta)$ increases with the increase of the local micro-rotation parameter K_1. On the other hand, micro-rotation velocity $G(\eta)$ decreases whenever the local micro-rotation parameter k1 increases as depicted in Figures 12–14 represent the effect of m on stream function $f(\eta)$ and velocity $f'(\eta)$. As m increases the stream function $f(\eta)$ and velocity $f'(\eta)$ increases. Even so with the increase of m temperature $\theta(\eta)$ and micro-rotation velocity $G(\eta)$ decreases as disposed of in Figures 15 and 16.

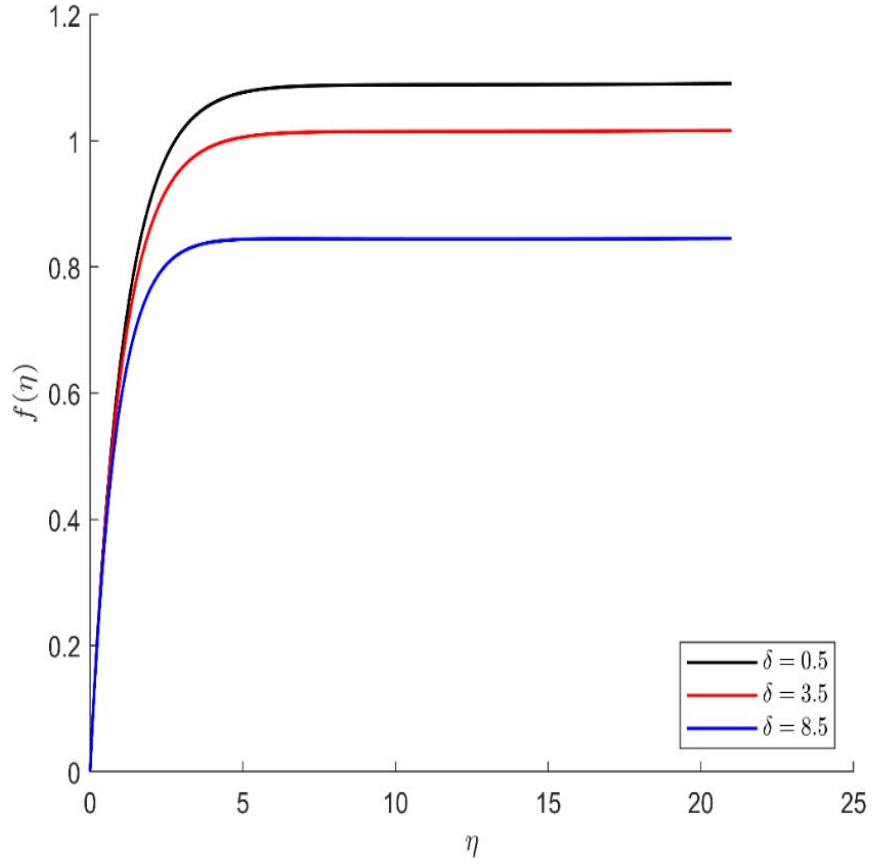

Figure 3. Representation of stream function $f(\eta)$ for the different values of δ with R = 5, n = 3, K =0.3, Pr = 0.6, ϕ_1 = 0.5, ϕ_2 = 0.03, m= 2.5, K_1 = 5.5, M = 1.

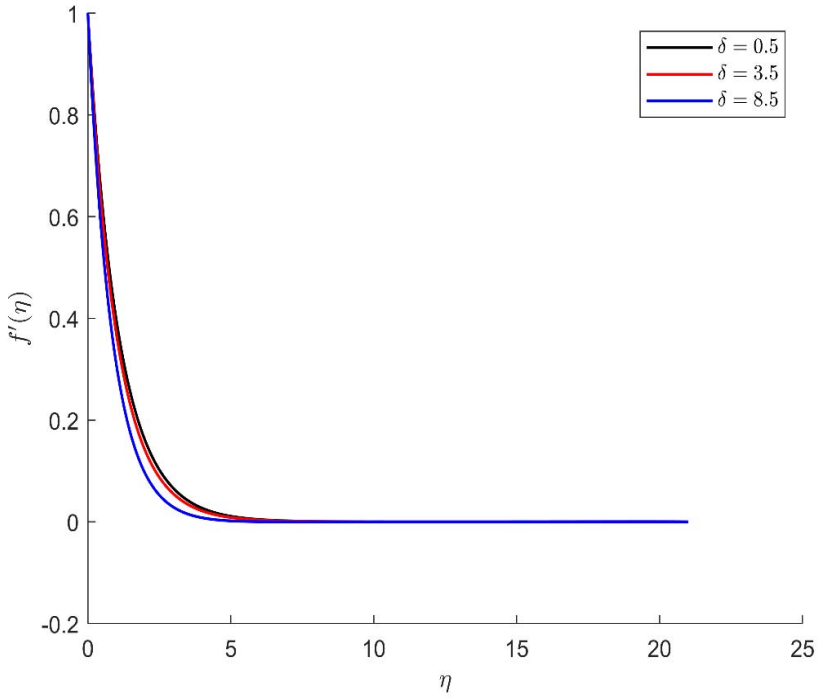

Figure 4. Representation of velocity $f'(\eta)$ for the different values δ with R = 5, n = 3, K =0.3, Pr = 0.6, ϕ_1 = 0.5, ϕ_2 = 0.03, m= 2.5, K_1 = 5.5, M = 1.

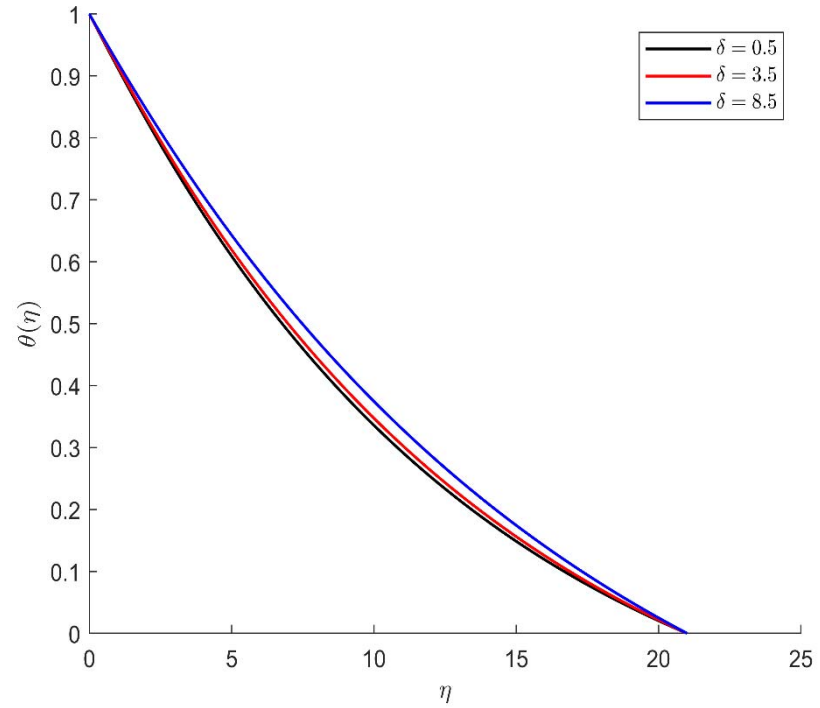

Figure 5. Representation of temperature $\theta(\eta)$ for the different values of δ with R = 5, n = 3, K =0.3, Pr = 0.6, ϕ_1 = 0.5, ϕ_2 = 0.03, m= 2.5, K_1 = 5.5, M = 1.

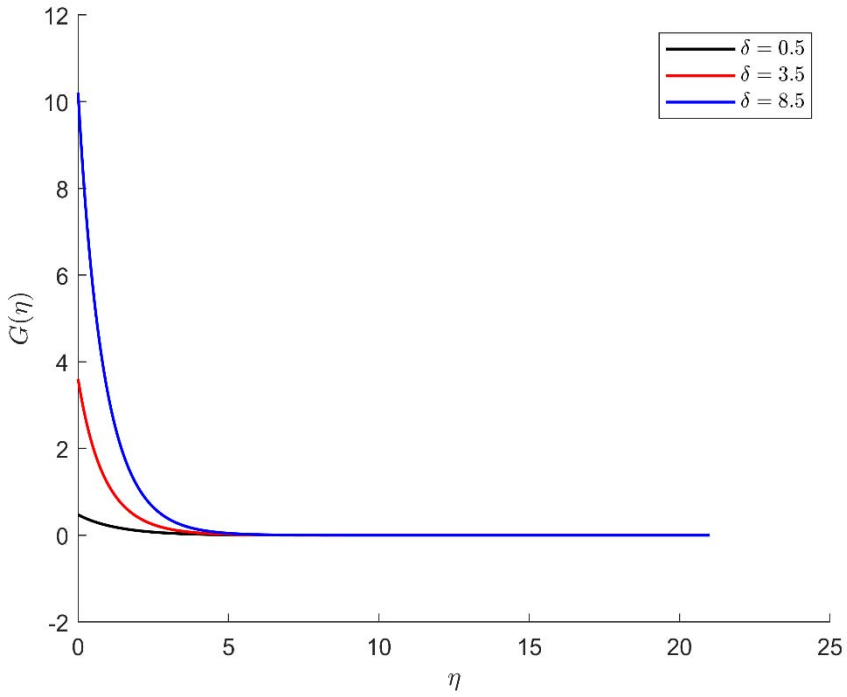

Figure 6. Representation of micro-rotation velocity $G(\eta)$ for the different values of δ with R = 5, n = 3, K =0.3, Pr = 0.6, ϕ_1 = 0.5, ϕ_2 = 0.03, m= 2.5, K_1 = 5.5, M = 1.

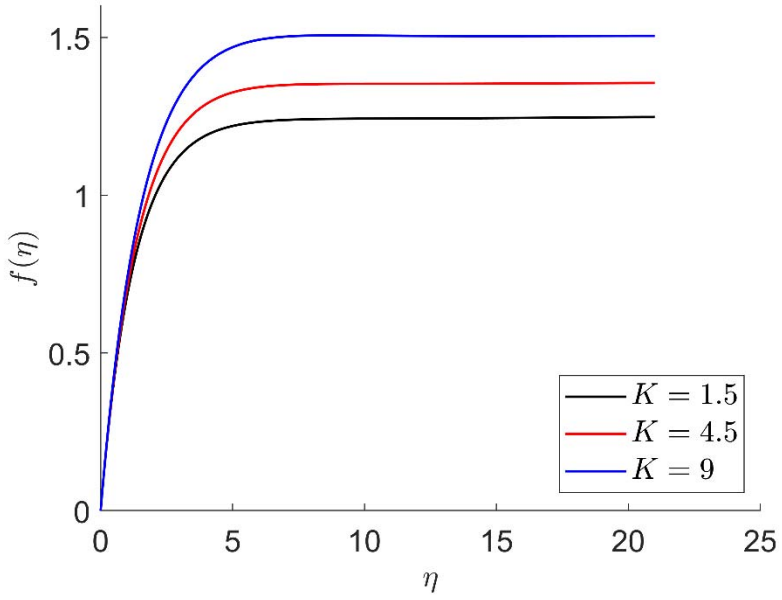

Figure 7. Representation of stream function $f(\eta)$ for the different values of micro-rotation parameter K, with R = 5, n =3, Pr = 0.6, ϕ_1 = 0.5, ϕ_2 = 0.02, m = 5, K_1 = 5.5, delta = 0.5, M = 1.

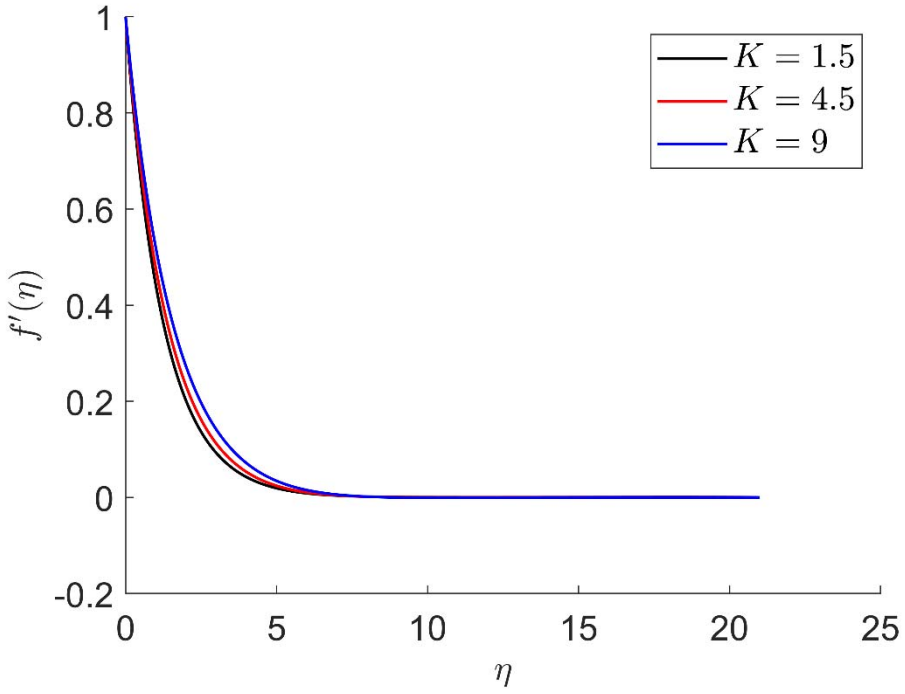

Figure 8. Representation of velocity $f'(\eta)$ for the different values of micro-rotation parameter K, with R = 5, n =3, Pr = 0.6, ϕ_1 = 0.5, ϕ_2 = 0.02, m = 5, K_1 = 5.5, δ = 0.5, M = 1.

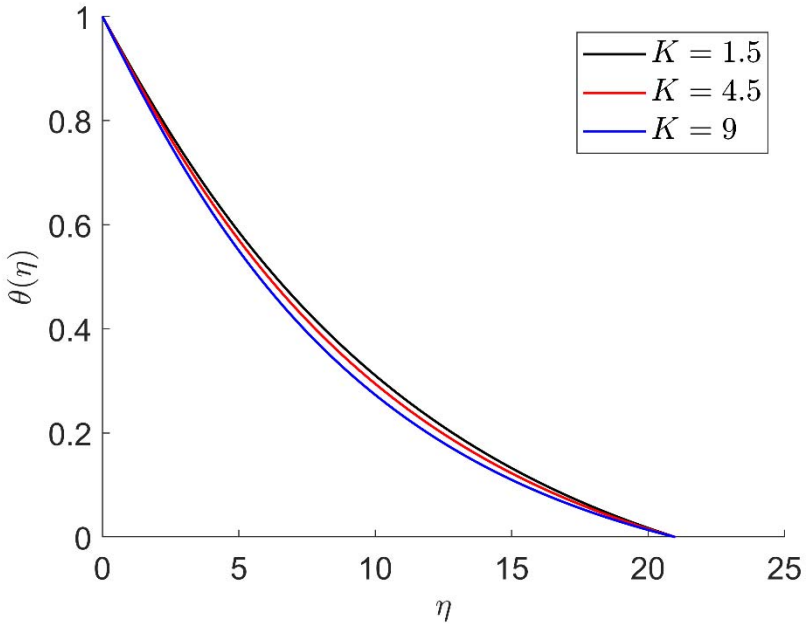

Figure 9. Representation of temperature $\theta(\eta)$ for the different values of micro-rotation parameter K, with R = 5, n =3, Pr = 0.6, ϕ_1 = 0.5, ϕ_2 = 0.02, m = 5, K_1 = 5.5, δ = 0.5, M = 1.

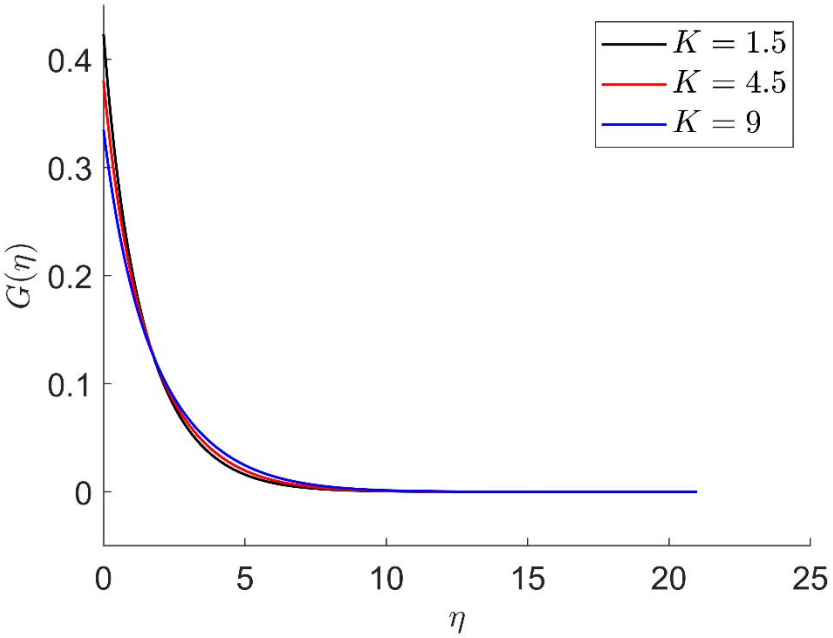

Figure 10. Representation of micro-rotation velocity $G(\eta)$ for the different values of micro-rotation parameter K, with R = 5, n =3, Pr = 0.6, ϕ_1 = 0.5, ϕ_2 = 0.02, m = 5, K_1 = 5.5, δ = 0.5, M = 1.

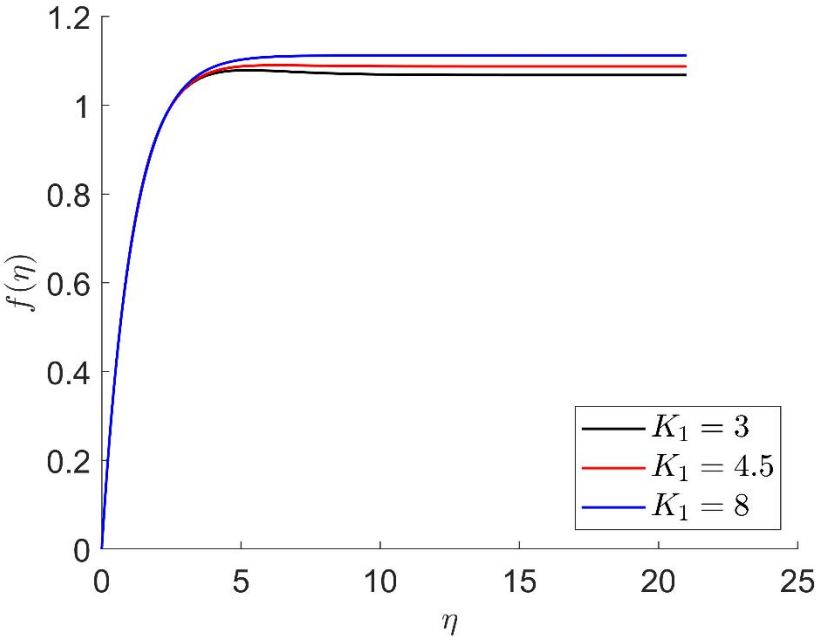

Figure 11. Representation of stream function $f(\eta)$ for the different values of the local micro-rotation parameter K_1, with R = 2.5, n = 3, K = 6, Pr = 0.9, ϕ_1 = 0.5, ϕ_2 = 0.06, m = 1.5, δ = 0.7, M = 1.

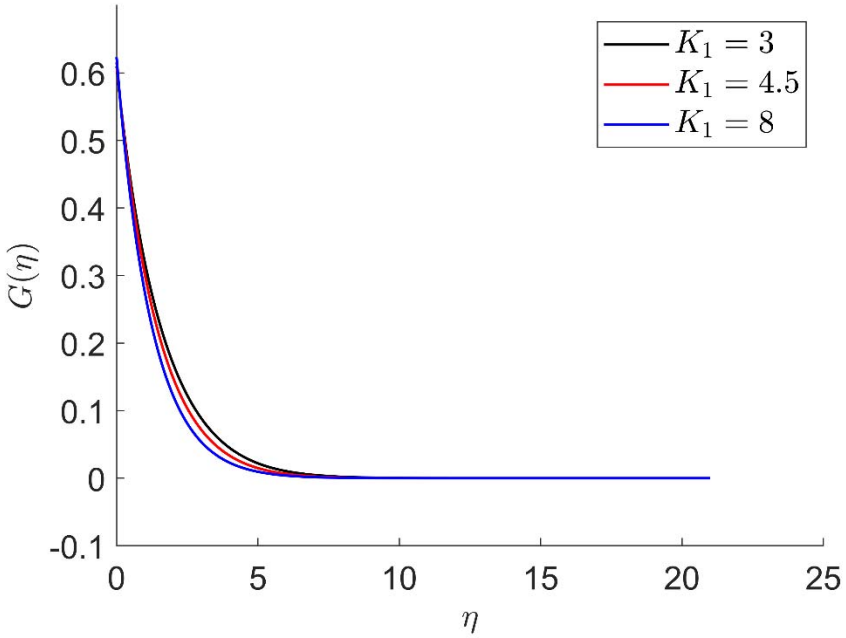

Figure 12. Representation of micro-rotation velocity $G(\eta)$ for the different values of the local micro-rotation parameter K_1, with R = 2.5, n = 3, K = 6, Pr = 0.9, ϕ_1 = 0.5, ϕ_2 = 0.06, m = 1.5, δ = 0.7, M = 1.

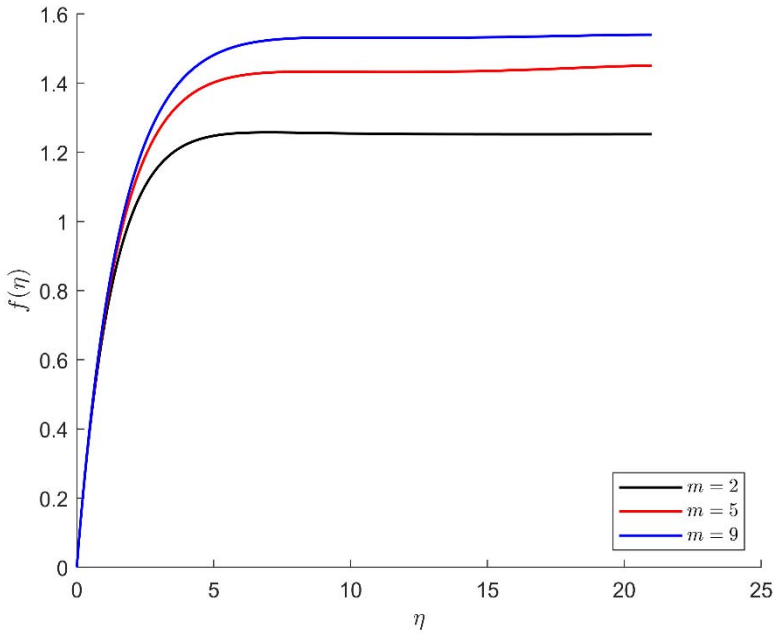

Figure 13. Representation of stream function $f(\eta)$ for the different values of m, with R = 1, n = 3, K = 5, Pr = 0.8, ϕ_1 = 0.5, ϕ_2 = 0.05, K_1 = 1.5, δ = 0.3, M = 1.

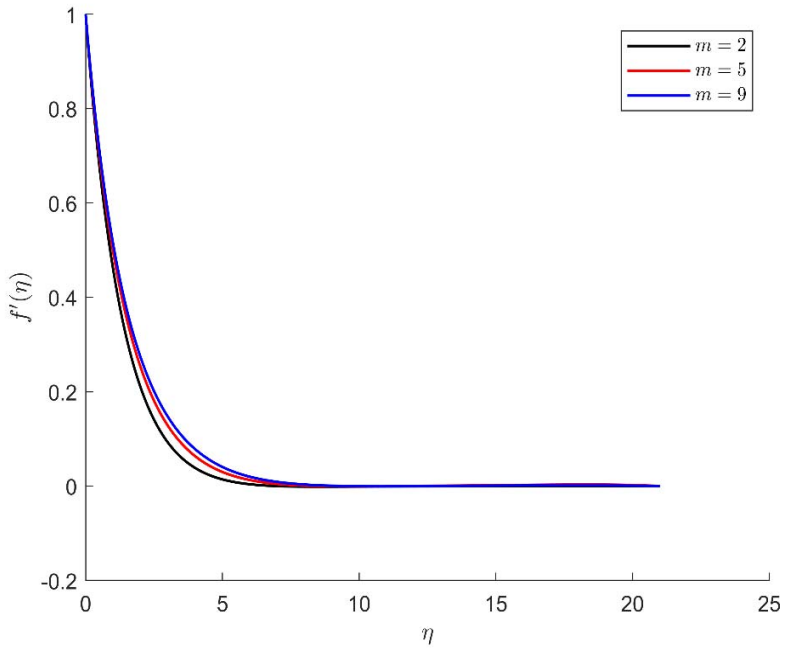

Figure 14. Representation of velocity $f'(\eta)$ for the different values of m, with R = 1, n = 3, K = 5, Pr = 0.8, ϕ_1 = 0.5, ϕ_2 = 0.05, K_1 = 1.5, δ = 0.3, M = 1.

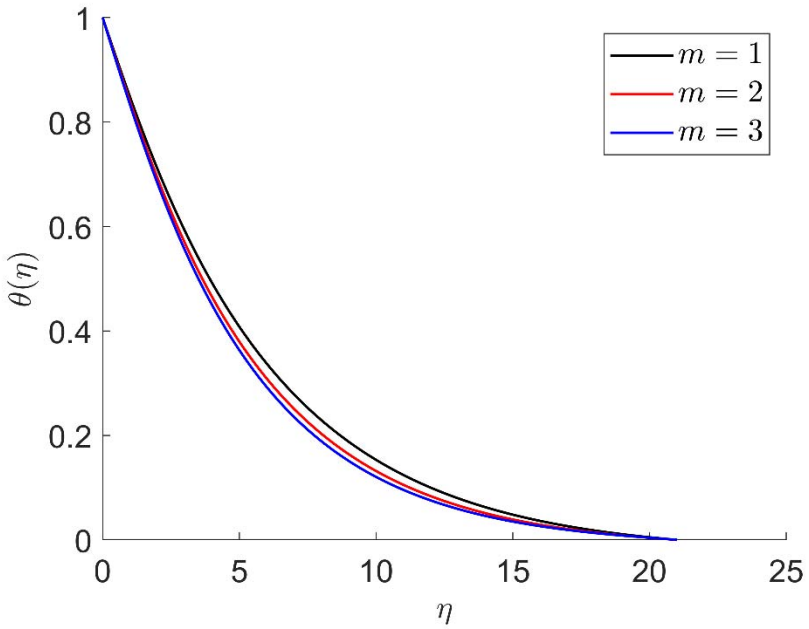

Figure 15. Representation of temperature $\theta(\eta)$ for the different values of m, with R = 1, n = 3, K = 5, Pr = 0.8, ϕ_1 = 0.5, ϕ_2 = 0.05, K_1 = 1.5, δ = 0.3, M = 1.

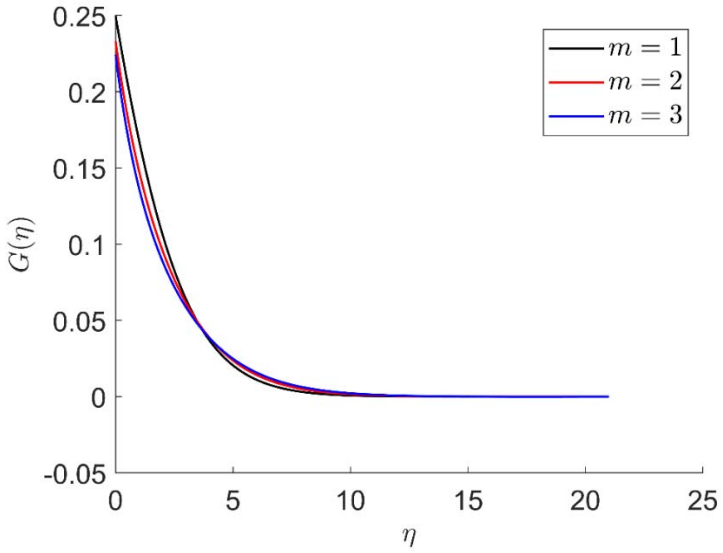

Figure 16. Representation of micro-rotation velocity $G(\eta)$ for the different values of m, with R = 1, n = 3, K = 5, Pr = 0.8, ϕ_1 = 0.5, ϕ_2 = 0.05, K_1 = 1.5, δ = 0.3, M = 1.

Figures 17–20 are created to represent the effects of magnetic parameters on stream function $f(\eta)$ and velocity $f'(\eta)$, temperature $\theta(\eta)$ and micro-rotation velocity $G(\eta)$ respectively, under the presumption that the other parameters have default values. When M increases then stream function $f(\eta)$ and velocity $f'(\eta)$ decrease display in Figures 17 and 18. The velocity field decreases as greater resistance to the flow phenomena is created by the application of the applied magnetic field. So, it is seen that the stream function $f(\eta)$ and velocity curve $f'(\eta)$ are reduced as a result of the Magnetic improvement. In contrast increases for temperature profile $\theta(\eta)$ and micro-rotation velocity $G(\eta)$ as present in Figures 19 and 20. Magnetic materials experience a change in flux density as their temperature increases and decreases from an ambient temperature. Figure 21 illustrates the effect of shape factor n on temperature $\theta(\eta)$. When n = 3, 6.3698 and 16.1576 then its sphere, cylinder, and laminar respectively. Figures 22–24 exhibit the operation of ϕ_1 on-stream function $f(\eta)$, velocity $f'(\eta)$ temperature $\theta(\eta)$ increase with the value ϕ_1 increases. Unlike for micro-rotation velocity $G(\eta)$ in Figure 25. Stream function $f(\eta)$ and velocity $f'(\eta)$ are decrease as well as increase the value of ϕ_2 as present in Figures 26 and 27. Whereas in Figures 28 and 29 illustrate temperature $\theta(\eta)$ and micro-rotation velocity $G(\eta)$ increase when increasing the value of ϕ_2. Figures 22–29 show, the effects of the solid volume fractions of Alumina/Aluminum oxide and Copper/Copper on the thermal field. The volume fraction of Alumina/Aluminium oxide and Cuprum/Copper are boosting the thermal phenomena. However, as compared to ϕ_1, the thermal profiles in case of ϕ_2 are more obvious. Due to the nanoparticle volume fractions, the behaviour of these figures is consistent with the physical behaviour of the nanofluid. The thermal conductivity of the nanoparticles is greater than that of the base fluid, which increases the total thermal conductivity of the nanofluid and contributes to the rise in boundary layer temperature. Figure 30 display that as the Prandtl number increases the temperature $\theta(\eta)$ decrease. It is evident that the temperature distribution is a decreasing function of Prandtl number. This is because the thermal diffusivity of the fluid decreases due to higher values of Pr which further led the reduction in the thermal boundary layer thickness. The impact of radiation factors on temperature $\theta(\eta)$ are examined in Figure 31. More heat is introduced to the thermal phenomena as a result of changing the radiation parameter. More heat is

introduced to the thermal phenomena as a result of changing the radiation parameter. As a result, the temperature curves are increased by the increasing radiation parameter value. Physically, by raising the value of the parameter R, we may enhance the radiative heat transfer.

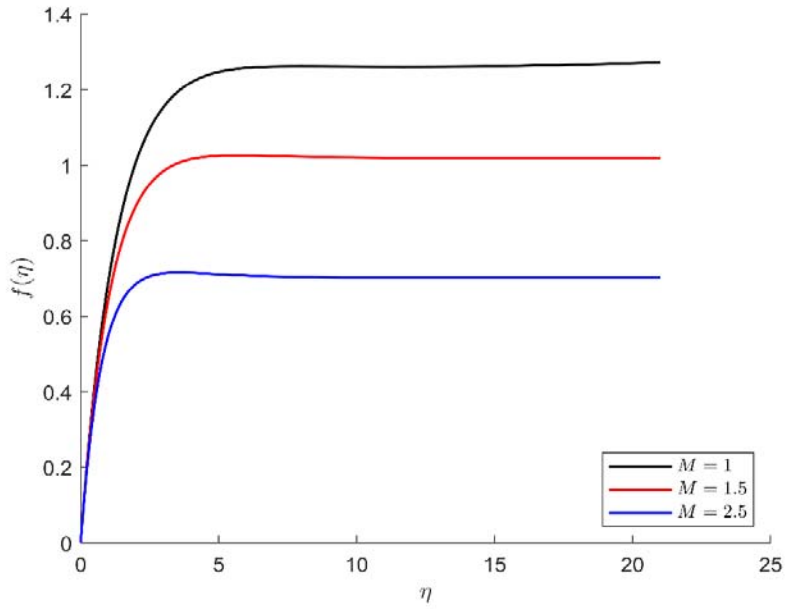

Figure 17. Representation of stream function $f(\eta)$ for the different values of M, with R = 2, n = 1, K = 3, Pr = 0.6, ϕ_1 = 0.5, ϕ_2 = 0.01, m = 3.5, K_1 = 2, δ =0.4.

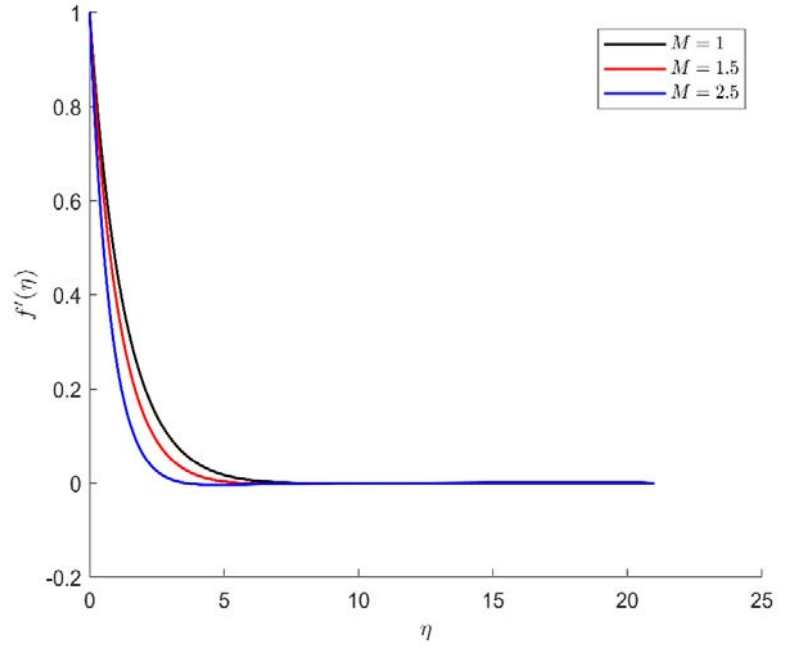

Figure 18. Representation of velocity $f'(\eta)$ for the different values of M, with R = 2, n = 1, K = 3, Pr = 0.6, ϕ_1 = 0.5, ϕ_2 = 0.01, m = 3.5, K_1 = 2, δ =0.4.

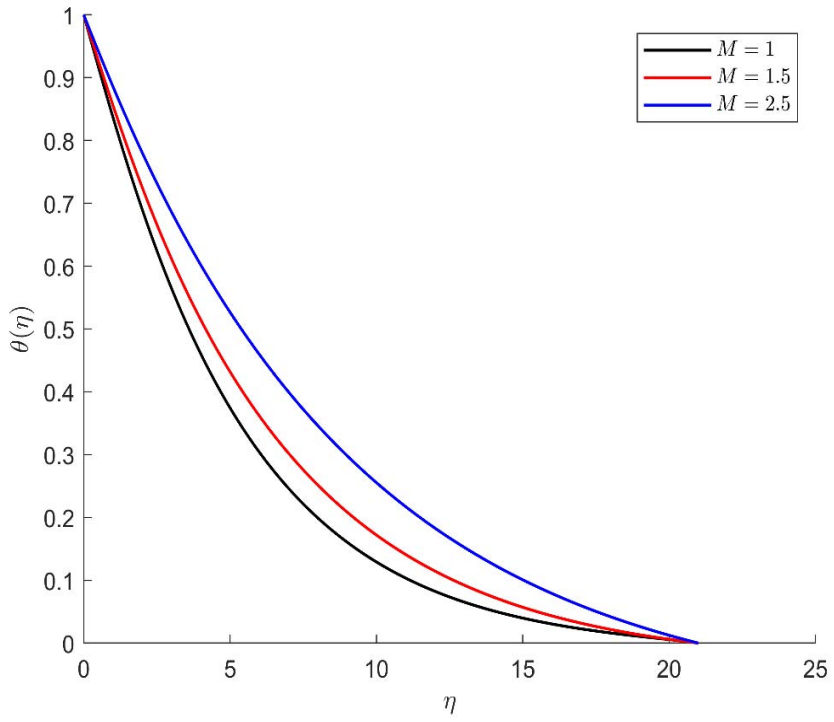

Figure 19. Representation of temperature $\theta(\eta)$ for the different values of M, with R = 2, n = 1, K = 3, Pr = 0.6, ϕ_1 = 0.5, ϕ_2 = 0.01, m = 3.5, K_1 = 2, δ =0.4.

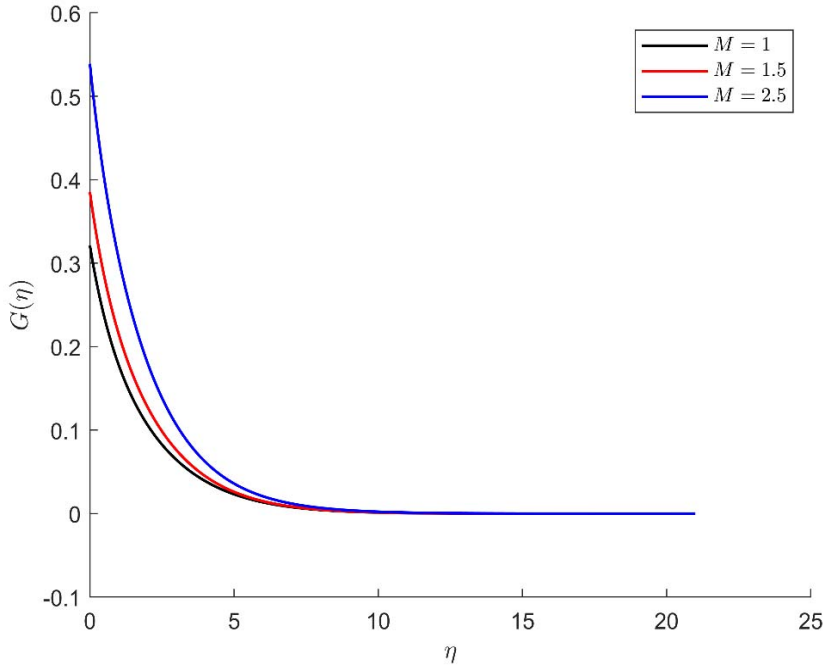

Figure 20. Representation of micro-rotation velocity $G(\eta)$ for the different values of M, with R = 2, n = 1, K = 3, Pr = 0.6, ϕ_1 = 0.5, ϕ_2 = 0.01, m = 3.5, K_1 = 2, δ =0.4.

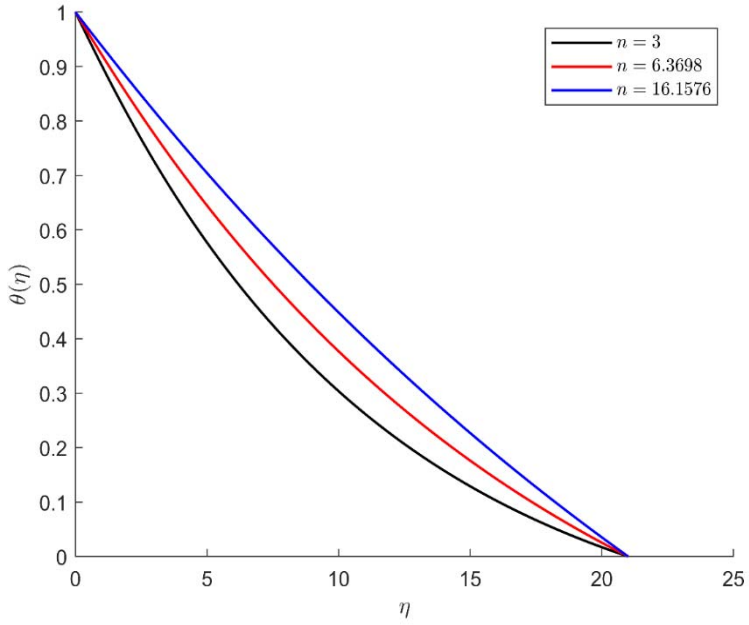

Figure 21. Representation of temperature $\theta(\eta)$ for the different values of shape factor n, with R = 2, K = 3, Pr = 0.6, ϕ_1 = 0.5, ϕ_2 = 0.01, m = 3.5, K_1 = 2, δ = 0.4, M = 2.

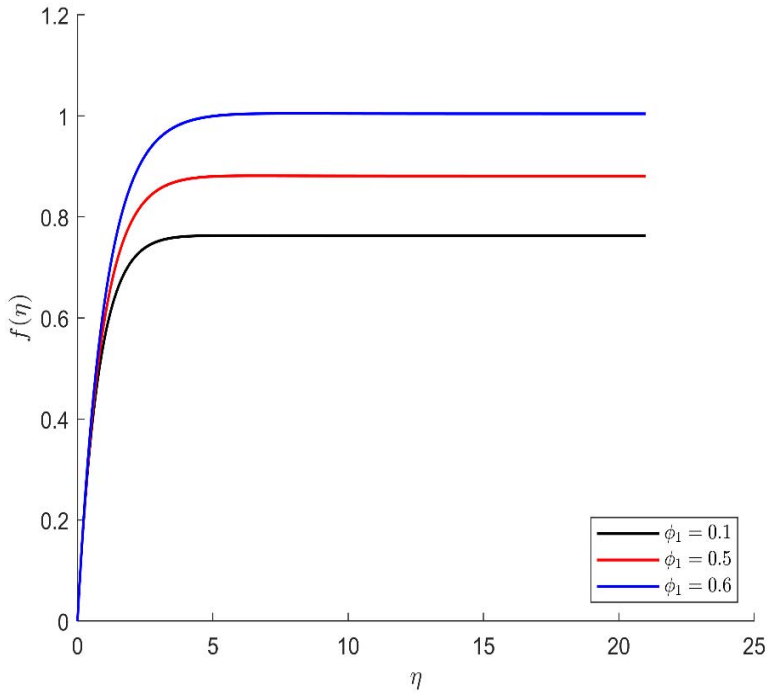

Figure 22. Representation of stream function $f(\eta)$ for the different values of ϕ_1, with R = 6, n = 2, K = 1, Pr = 0.6, ϕ_2 = 0.02, m = 5, K_1 = 2.5, δ = 0.2, M =2.

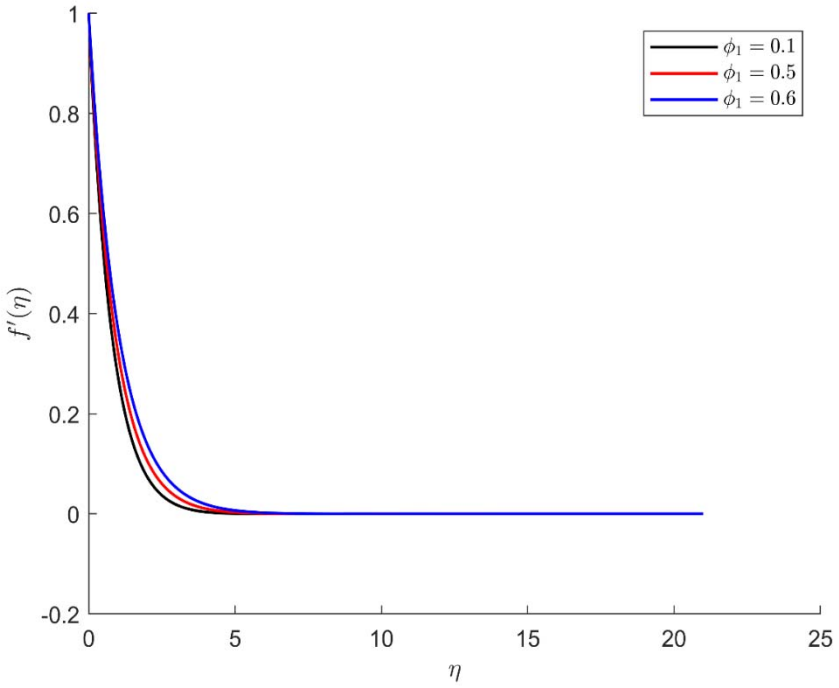

Figure 23. Representation of velocity $f'(\eta)$ for the different values of ϕ_1, with R = 6, n = 2, K = 1, Pr = 0.6, ϕ_2 = 0.02, m = 5, K_1 = 2.5, δ = 0.2, M = 2.

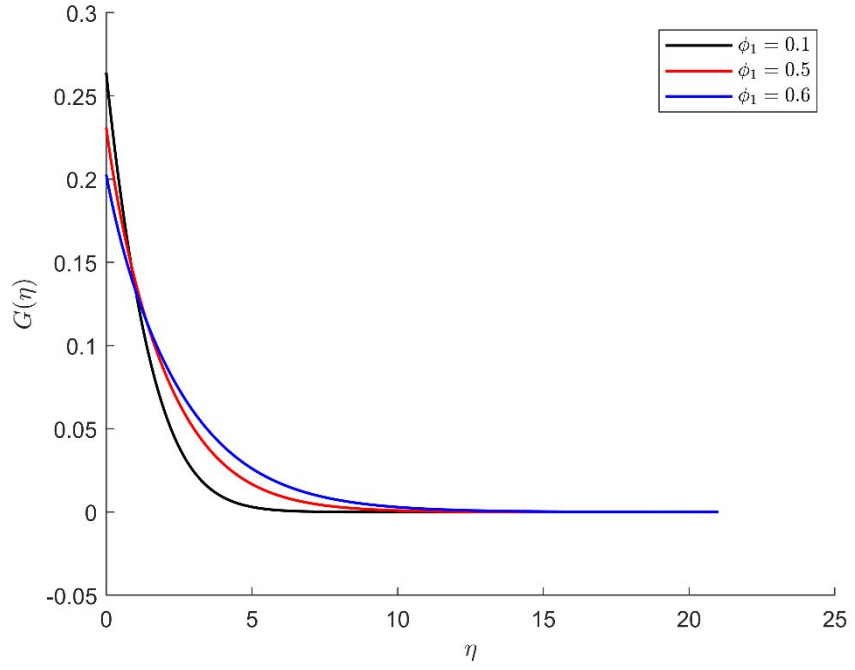

Figure 24. Representation of micro-rotation velocity $G(\eta)$ for the different values of ϕ_1, with R = 6, n = 2, K = 1, Pr = 0.6, ϕ_2 = 0.02, m = 5, K_1 = 2.5, δ = 0.2, M =2.

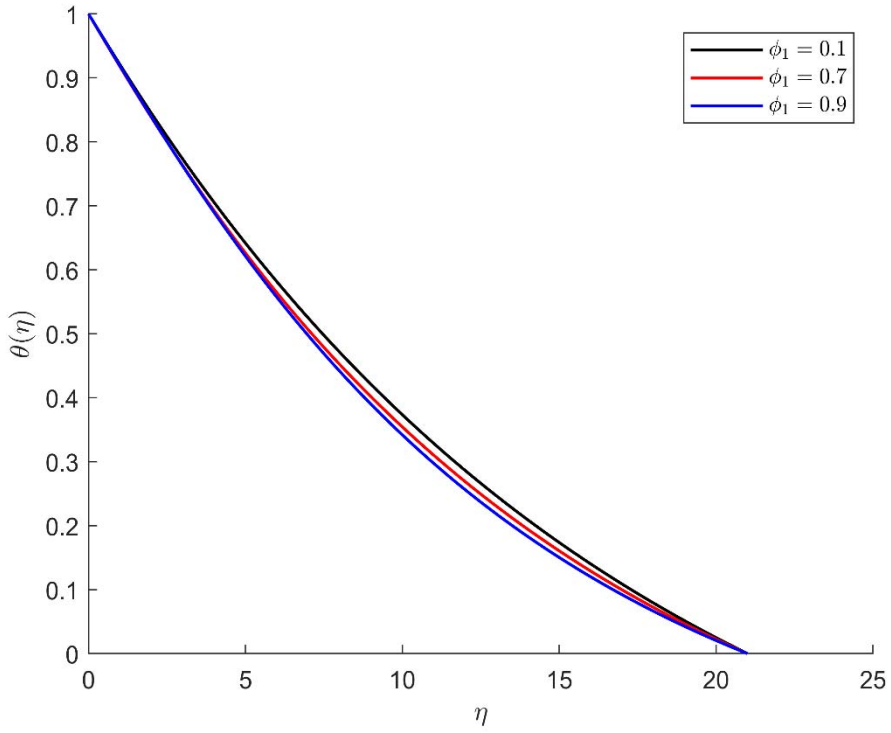

Figure 25. Representation of temperature $\theta(\eta)$ for the different values of ϕ_1, with R = 6, n = 2, K = 1, Pr = 0.6, ϕ_2 = 0.02, m = 5, K_1 = 2.5, δ = 0.5, M = 2.

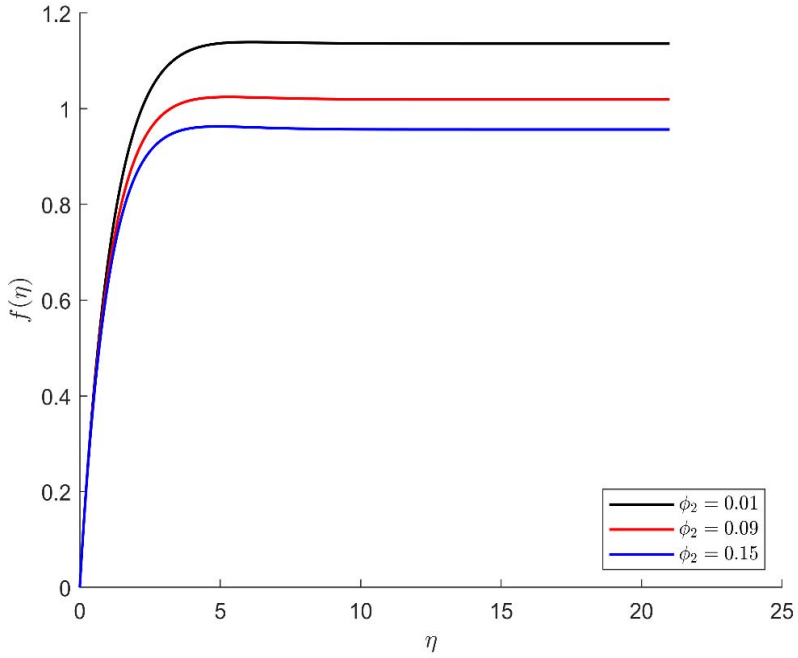

Figure 26. Representation of stream function $f(\eta)$ for the different values of ϕ_2, with R = 3, n = 5, K = 6, Pr = 0.8, ϕ_1 = 0.1, m = 3, K_1 = 2.5, δ = 0.2, M = 2.

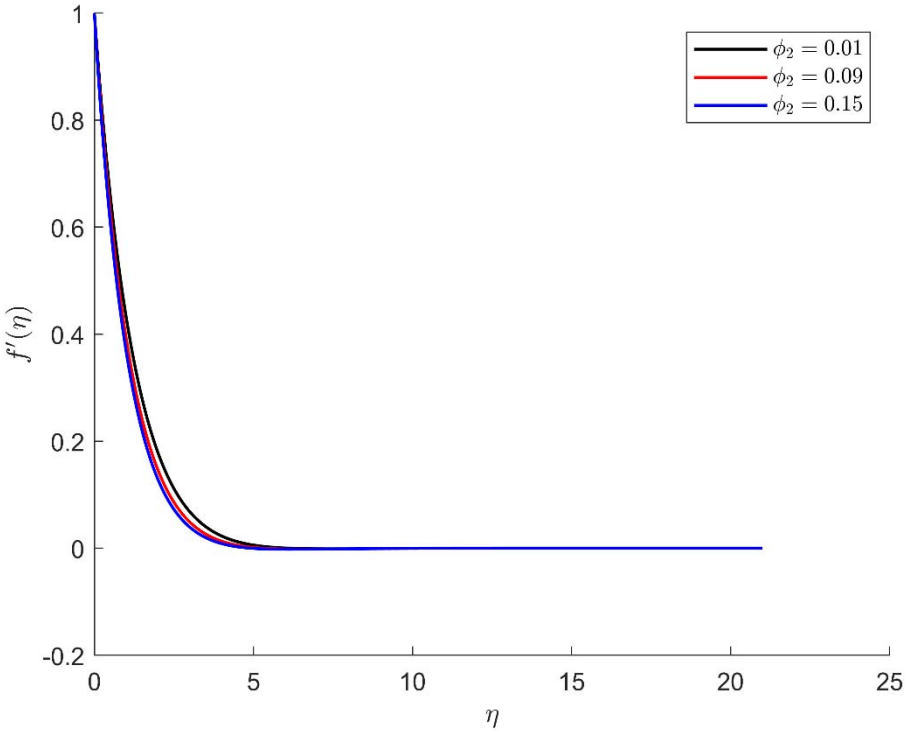

Figure 27. Representation of velocity $f'(\eta)$ for the different values of ϕ_2, with R = 3, n = 5, K = 6, Pr = 0.8, ϕ_1 = 0.1, m = 3, K_1 = 2.5, delta = 0.2, δ = 5, M = 2.

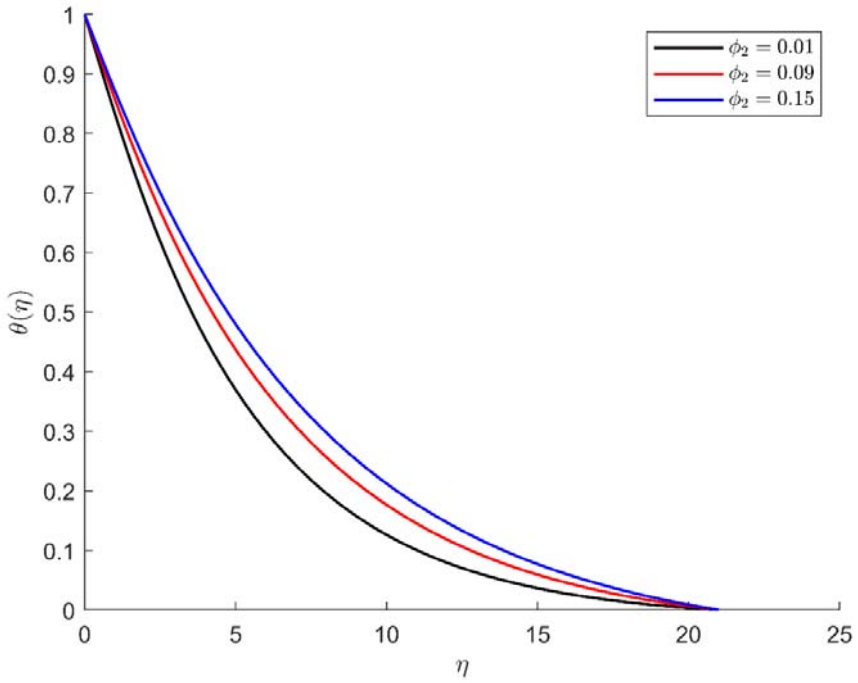

Figure 28. Representation of temperature $\theta(\eta)$ for the different values of ϕ_2, with R = 3, n = 5, K = 6, Pr = 0.8, ϕ_1 = 0.1, m = 3, K_1 = 2.5, δ = 0.2, M = 2.

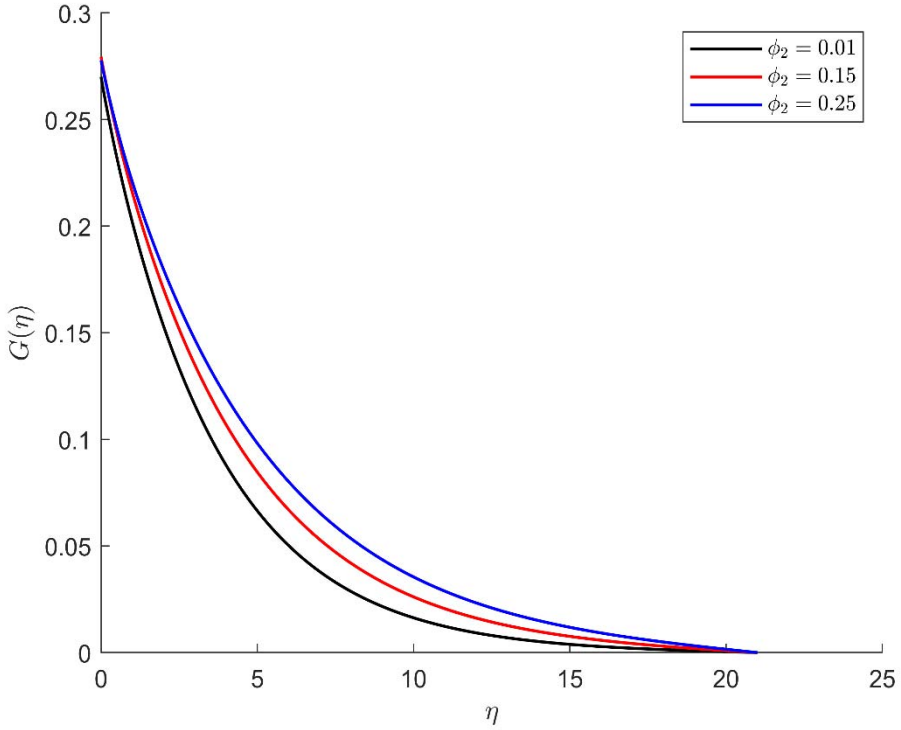

Figure 29. Representation of micro-rotation velocity $G(\eta)$ for the different values of ϕ_2, with R = 3, n = 5, K = 6, Pr = 0.8, ϕ_1 = 0.7, m = 5, K_1 = 2.5, δ = 0.2, M = 4.

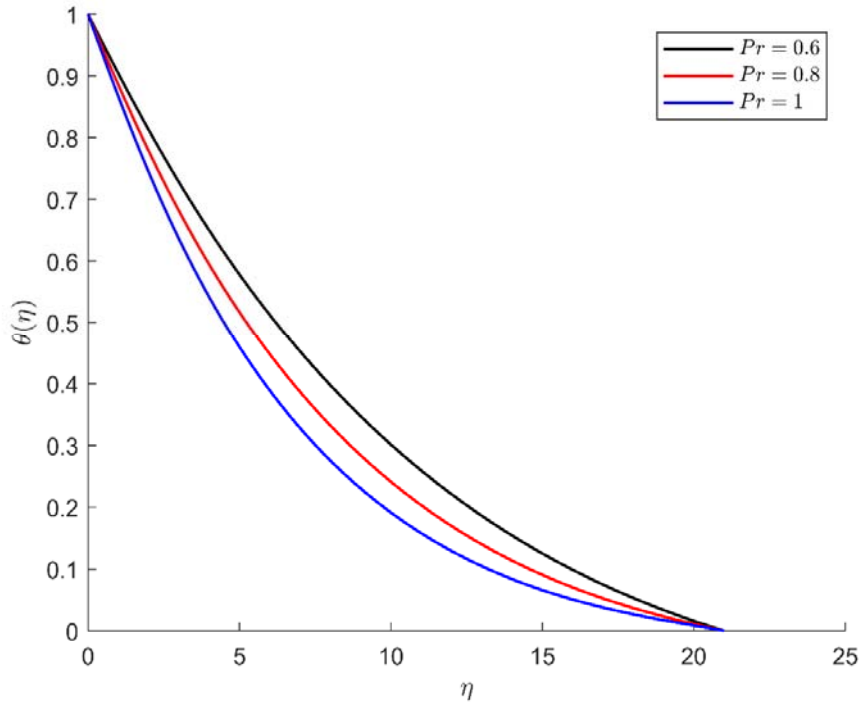

Figure 30. Representation of temperature $\theta(\eta)$ for the different values of Prandtl number, with R = 6, n = 3, K = 2, ϕ_1 = 0.2, ϕ_2 = 0.02, m = 5, K_1 = 2.5, δ = 0.2, M = 1

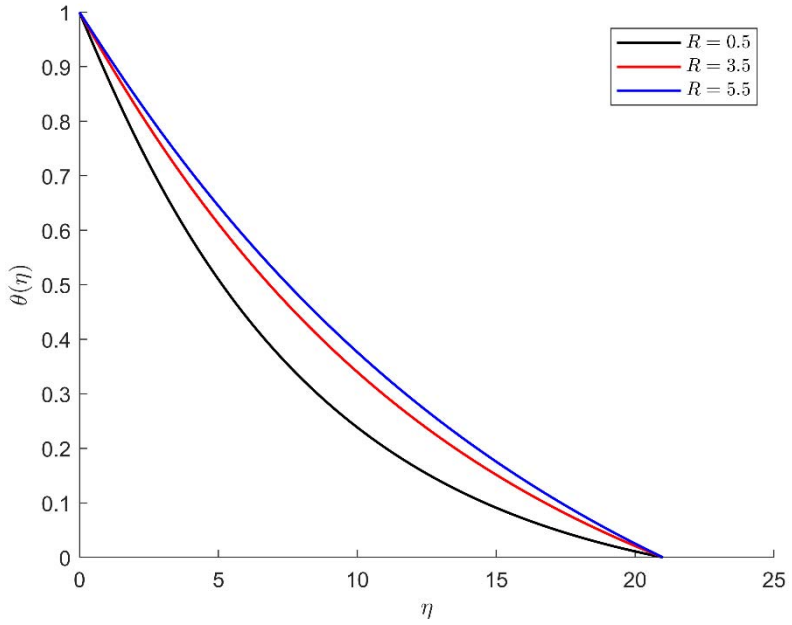

Figure 31. Representation of temperature $\theta(\eta)$ for the different values of R, with n = 3, K = 1, Pr = 0.6, ϕ_1 = 0.5, ϕ_2 = 0.01, m = 5, K_1 = 6.5, δ = 0.5, M = 2.

The numerical outcomes of the Nusselt number, skin coefficient friction and Sherwood number are shown. The heat transfer factor is shown in Table 2 to see if the values of δ, Pr, ϕ_1, ϕ_2, Alpha, and M are inclined then heat transfer is also inclined. The effect of a different number of stretching parameters and other numbers on the skin coefficient friction is numerically shown in Table 2. When the quantities of δ, Pr, and M increase then skin coefficient friction expands, and if K_1 expands, and the skin coefficient friction declines. The effect of M, Pr, K_1, and δ, ϕ_1, ϕ_2, on the Sherwood number is shown in Table 3. If the value of K_1 increases, then the mass transfer rate decreases. When the values M, m, K, and δ increase then the mass flow rate increase. The effect of various parameters δ, Pr, R, n, K_1 and M on Nusselt number has been depicted in Table 4. It has been observed that when the values of parameters δ, M, R and N increase then the heat transfer expands, and if k, Pr and K_1 expand, the Nusselt number decline.

Table 5 provides the comparative study of hybrid nanofluid and nanofluid under the effect of magnetic parameter M on Nusselt number, Skin friction, and Sherwood number. It is observed that the Nusselt number or heat transfer rate and shear stress or skin friction and Sherwood number or surface mass flux of hybrid nanofluid are better as compared to nanofluid flow.

Table 6 offers the proportional study of hybrid nanofluid and nanofluid under the effect of boundary parameter δ on Nusselt number, Skin friction, and Sherwood number. It is detected that the Nusselt number or heat transfer rate and shear stress or skin friction and Sherwood number or surface mass flux of hybrid nanofluid are better as compared to nanofluid flow. The values of other parameters in Tables 5 and 6 are taken as $Rd = 1.2$, $R = 3$, $n = 3$, $K = 6$, $Pr = 0.8$, $m = 3$, $K_1 = 2.5$, $\delta = 0.2$, $\alpha = 5$, $M = 2$.

In the comparison Tables 5 and 6, we have considered (a) $\phi_1 = 0.2$ and $\phi_2 = 0$ in the case of nanofluid (b) $\phi_1 = 0.1$ and $\phi_2 = 0.1$ in the case of hybrid nanofluid, where $Al_2O_3 \rightarrow \phi_1$ and $Cu \rightarrow \phi_2$.

Table 2. Variation of $C_f(Re_x)^{-(1/2)}$ for a discrete number of parameters.

δ	R	N	K	Pr.	ϕ_1	ϕ_2	m	K_1	α	M	$f''(\eta)$
0.5	5	3	0.3	0.6	0.5	0.03	2.5	5.5	2.5	1	–0.000976
3.5											–0.000699
8.5											0.000222
0.5	0.5	3	1	0.6	0.5	0.01	5	6.5	2.8	2	0.000165
	3.5										0.000165
	5.5										0.0001653
0.4	2	3	3	0.6	0.5	0.01	3.5	2	1	2	0.003354
		6.3698									0.003354
		16.1576									0.003354
0.5	5	3	1.5	0.6	0.5	0.02	5	5.5	2	1	–0.001637
			4.5								–0.000945
			9								–0.000448
0.2	6	3	2	0.6	0.2	0.02	5	2.5	3	1	–0.000035
				0.8							–0.000035
				1							–0.000035
0.2	6	2	1	0.6	0.1	0.02	5	2.5	3	2	0.000122
					0.5						0.000610
					0.6						0.000374
0.2	3	5	6	0.8	0.1	0.01	3	2.5	5	2	0.001575
						0.09					0.001711
						0.15					0.001724
0.3	1	3	5	0.8	0.5	0.05	1	1.5	2	1	0.000002
							2				–0.000330
							3				–0.001959
0.7	2.5	3	6	0.9	0.5	0.06	1.5	3	2	1	0.003838
								4.5			0.001401
								8			–0.000379
0.4	2	1	3	0.6	0.5	0.01	3.5	2	1	1	0.000838
										1.5	0.002978
										2.5	0.003277

Table 3. Variation of $\mathrm{S}h_x(Re_x)^{-(1/2)}$ for a discrete number of parameters.

δ	R	N	K	Pr.	ϕ_1	ϕ_2	m	K_1	α	M	$G'(\eta)$
0.5	5	3	0.3	0.6	0.5	0.03	2.5	5.5	2.5	1	0.000637
3.5											0.000821
8.5											0.001262
0.5	0.5	3	1	0.6	0.5	0.01	5	6.5	2.8	2	0.000525
	3.5										0.000525
	5.5										0.000525
0.4	2	3	3	0.6	0.5	0.01	3.5	2	1	2	0.003126
		6.3698									0.003126
		16.1576									0.003126
0.5	5	3	1.5	0.6	0.5	0.02	5	5.5	2	1	0.001389
			4.5								0.001874
			9								0.002749
0.2	6	3	2	0.6	0.2	0.02	5	2.5	3	1	0.000410
				0.8							0.000410
				1							0.000410
0.2	6	2	1	0.6	0.1	0.02	5	2.5	3	2	0.000037
					0.5						0.001691
					0.6						0.003608
0.2	3	5	6	0.8	0.1	0.01	3	2.5	5	2	0.000359
						0.09					0.000304
						0.15					0.000337
0.3	1	3	5	0.8	0.5	0.05	1	1.5	2	1	–0.000000
							2				0.000014
							3				0.000023
0.7	2.5	3	6	0.9	0.5	0.06	1.5	3	2	1	0.001164
								4.5			0.000586
								8			0.000470
0.4	2	1	3	0.6	0.5	0.01	3.5	2	1	1	0.002425
										1.5	0.002586
										2.5	0.003882

Table 4. Variation of $\mathrm{N}u_x(Re_x)^{-(1/2)}$ for the discrete number of parameters.

δ	R	N	k	Pr.	ϕ_1	ϕ_2	m	K_1	α	M	$\theta'(\eta)$
0.5	5	3	0.3	0.6	0.5	0.03	2.5	5.5	2.5	1	0.239779
3.5											0.245450
8.5											0.258792
0.5	0.5	3	1	0.6	0.5	0.01	5	6.5	2.8	2	0.179407
	3.5										0.229167
	5.5										0.246877
0.4	2	3	3	0.6	0.5	0.01	3.5	2	1	2	0.211021
		6.3698									0.246739
		16.1576									0.282326
0.5	5	3	1.5	0.6	0.5	0.02	5	5.5	2	1	0.221892
			4.5								0.214110
			9								0.203964
0.2	6	3	2	0.6	0.2	0.02	5	2.5	3	1	0.067710
				0.8							0.058471
				1							0.050255
0.2	6	2	1	0.6	0.1	0.02	5	2.5	3	2	0.428781
					0.5						0.433304
					0.6						0.429139
0.2	3	5	6	0.8	0.1	0.01	3	2.5	5	2	0.040132
						0.09					0.049593
						0.15					0.055833
0.3	1	3	5	0.8	0.5	0.05	1	1.5	2	1	0.014491
							2				0.012162
							3				0.013738
0.7	2.5	3	6	0.9	0.5	0.06	1.5	3	2	1	0.180677
								4.5			0.179365
								8			0.177359
0.4	2	1	3	0.6	0.5	0.01	3.5	2	1	1	0.120237
										1.5	0.144988
										2.5	0.186923

Table 5. Comparison of nanofluid and hybrid nanofluid flow for different values of magnetic parameter M.

Parameter	Skin Friction C_f		Nusselt Number N_u		Sherwood Number Sh	
M	$Al_2O_3 - EG$	$Al_2O_3 - C_u/EG$	$Al_2O_3 - EG$	$Al_2O_3 - C_u/EG$	$Al_2O_3 - EG$	$Al_2O_3 - C_u/EG$
3	–1.7899	–2.3778	–0.1511	–0.1947	0.1326	0.1301
4	–2.2672	–2.9818	–0.2240	–0.2711	0.1132	0.1118
5	–2.7581	–3.6074	–0.3036	–0.3540	0.1001	0.0992

Table 6. Comparison of nanofluid and hybrid nanofluid flow for different values of boundary parameter δ.

Parameter	Skin Friction C_f		Nusselt Number N_u		Sherwood Number Sh	
δ	$Al_2O_3 - EG$	$Al_2O_3 - C_u/EG$	$Al_2O_3 - EG$	$Al_2O_3 - C_u/EG$	$Al_2O_3 - EG$	$Al_2O_3 - C_u/EG$
0.1	–1.2860	–1.7428	0.0829	0.0651	0.1660	0.1613
0.3	–1.4054	–1.9044	–0.2762	–0.3400	0.1563	0.1515
0.5	–1.5478	–2.0970	–0.6996	–0.8162	0.1437	0.1387

5. Conclusions

In this study, the microstructure and inertial characteristics of a magnetite ferrofluid over a non-linearly stretching sheet using the BVP4c method are examined. The effect of related parameters on stream function, velocity, micro-rotation velocity, and temperature are demonstrated graphically. Results revealed that:

(1) On the stream function subject, there is an inverse relation between magnetic and micro-rotation parameters.

(2) On the velocity subject, there is a reverse relation between boundary and micro-rotation parameters.

(3) On the micro-rotation velocity subject, in the deficiency of magnetic parameter, micro-rotation velocity is in the lowest form.

(4) On the temperature subject, the highest temperature is attained for the lowest value of the micro-rotation parameter.

The work done in this article can be extended for other non-Newtonian fluids, like, Maxwell fluid, Second grade fluid, and Oldroyd-B fluid, etc.

Nomenclature	
I Body couple per unit mass	σ_s Ferroparticles electric conductivity $\boldsymbol{S/m}$
u x-component of velocity $\boldsymbol{m/s}$	B_0 Magnetic field intensity W/m^2
ϕ, λ Spin gradient viscosity coefficients $\boldsymbol{Pa.s}$	F'' Coefficient of skin-friction
j Micro-inertia density $\boldsymbol{Kg/m^3}$	σ_{nf} Ferrofluid electric conductivity S/m
v y-component of velocity $\boldsymbol{m/s}$	$C_{p,nf}$ Ferrofluid heat capacity
μ_f Base fluid dynamic viscosity $\boldsymbol{Pa.s}$	G Dimensionless micro-rotation velocity m/s
K Micro-rotation parameter	σ^* Stefan-Boltzmann constant
V Velocity $\boldsymbol{m/s}$	g Acceleration due to gravity
μ_{nf} Ferrofluid dynamic viscosity $\boldsymbol{Kg/ms}$	θ Dimensionless temperature
	f Base fluid

Continued on next page

k^* Mean absorption coefficient	p Pressure $Kgm^{-1}s^{-2}$
T The temperature of the fluid (°C)	ρ_f Base fluid density Kg/m^3
ϕ Ferroparticles volume fraction	s Ferroparticle
k_f Base fluid thermal conductivity $\boldsymbol{Wm^{-1}K^{-1}}$	Pr Prandtl number m^2/s
T_w Wall temperature	ρ_s Ferroparticles density Kg/m^3
δ Boundary parameter	hnf hybrid Ferrofluid
k_s Ferroparticle thermal conductivity $\boldsymbol{Wm^{-1}K^{-1}}$	q_r Radiative heat flux
T_∞ Ambient temperature	ρ_{hnf} hybrid Ferrofluid density Kg/m^3
κ Vortex viscosity	w Condition at wall
k_{nf} Ferroparticle thermal conductivity $\boldsymbol{Wm^{-1}K^{-1}}$	R Radiative parameter α Stretching/shrinking parameter
F Dimensionless stream function	∞ Condition at infinity
f Base fluid electric conductivity $\boldsymbol{S/m}$	γ_{nf} Spin-gradient viscosity
N Micro-rotation vector	F' Dimensionless velocity $\boldsymbol{m/s}$
$\boldsymbol{K_1}$ local micro-rotation parameter	

Acknowledgments

This research received funding support from the NSRF via the Program Management Unit for Human Resources & Institutional Development, Research and Innovation, (grant number B05F650018).

Conflict of interest

The authors declare no conflict of interest.

References

1. S. U. S. Choi, J. Eastman, Enhancing thermal conductivity of fluids with nanoparticles, *Asme Fed,* **231** (1995), 99–103.
2. J. Buongiorno, D. C. Venerus, N. Prabhat, T. McKrell, J. Townsend, R. Christianson, et al., A benchmark study on the thermal conductivity of nanofluids, *J. Appl. Phys.*, **106** (2009), 094312. https://doi.org/10.1063/1.3245330
3. K. R. Singh, P. R. Solanki, B. D. Malhotra, A. C. Pandey, R. P. Singh, *Introduction to nanomaterials: An overview toward broad spectrum applications, nanomaterials in bionanotechnology,* CRC Press: Boca Raton, FL, USA, 2021. https://doi.org/10.1201/9781003139744-1

4. K. Suvardhan, C. Rajasekhar, R. Mashallah, *Smart nanodevices for point-of-care applications,* CRC Press: Boca Raton, FL, USA, 2021.
5. S. Upadhya, S. V. Mamatha, S. R. Raju, C. S. R. Raju, N. A. Shah, J. D. Chung, Importance of entropy generation on Casson, Micropolar and Hybrid magneto-nanofluids in a suspension of cross diffusion, *Chinese J. Phys.,* **77** (2022), 1080–1101. https://doi.org/10.1016/j.cjph.2021.10.016
6. Q. Lou, B. Ali, S. U. Rehman, D. Habib, S. Abdal, N. A. Shah, et al., Micropolar dusty fluid: Coriolis force effects on dynamics of MHD rotating fluid when Lorentz force is significant, *Mathematics*, **10** (2022), 2630. https://doi.org/10.3390/math10152630
7. Y. Li, M. Zhou, B. Cheng, Y. Shao, Recent advances in g-C3N4-based heterojunction photocatalysts, *J. Mater. Sci. Technol.,* **56** (2020), 1–17. https://doi.org/10.1016/j.jmst.2020.04.028
8. N. A. Shah, A. Wakif, E. R. El-Zahar, S. Ahmad, S-J. Yook, Numerical simulation of a thermally enhanced EMHD flow of a heterogeneous micropolar mixture comprising (60%)-ethylene glycol (EG), (40%)-water (W), and copper oxide nanomaterials (CuO), *Case Stud. Therm. Eng.,* 2022, 102046. https://doi.org/10.1016/j.csite.2022.102046
9. R. E. Rosensweig, *Ferrohydrodynamics*, Cambridge University Press, Cambridge, England, 1985.
10. S. U. S. Choi, D. A. Singer, H. P. Wang, Developments and applications of non-Newtonian flows, *Asme Fed,* **66** (1995), 99–105.
11. M. Hidetoshi, A. Ebata, K. Teramae, N. Hishiunma, Conductivity and viscosity of liquid by dispersed ultra-fine particles (dispersion of Al_2O_3, SiO_2, and TiO_2 ultra-fine particles), *Netsu Bussei,* **7** (1993). https://doi.org/10.2963/jjtp.7.227
12. M. Z. Ashraf, S. U. Rehman, S. Farid, A. K. Hussein, B. Ali, N. A. Shah, et al., Insight into significance of bioconvection on MHD tangent hyperbolic nanofluid flow of irregular thickness across a slender elastic surface, *Mathematics,* **10** (2022), 2592. https://doi.org/10.3390/math10152592
13. H. I. Andersson, O. A. Valnes, Flow of a heated ferrofluid over a stretching sheet in the presence of a magnetic dipole, *Acta Mech.,* **128** (1998), 39–47. https://doi.org/10.1007/BF01463158
14. H. I. Andersson, MHD flow of a viscoelastic fluid past a stretching surface, *Acta Mech.,* **95** (1992), 227–230. https://doi.org/10.1007/BF01170814
15. B. Gabriella, On similarity solutions of MHD flow over a nonlinear stretching surface in non-Newtonian power-law fluid, *Electron. J. Qual. Theo.*, **6** (2016), 1–12.
16. C. Fetecau, N. A. Shah, D. Vieru, General solutions for hydromagnetic free convection flow over an infinite plate with Newtonian heating, mass diffusion and chemical reaction, *Commun. Theor. Phys.*, **68** (2017), 768–782. https://doi.org/10.1088/0253-6102/68/6/768
17. A. S. Sabu, A. Wakif, S. Areekara, A. Mathew, N. A. Shah, Significance of nanoparticles' shape and thermo-hydrodynamic slip constraints on MHD alumina-water nanoliquid flows over a rotating heated disk: The passive control approach, *Int. Commun. Heat Mass Tran.,* **129** (2021), 105711. https://doi.org/10.1016/j.icheatmasstransfer.2021.105711.
18. G. Bognár, K. Hriczó, Ferrofluid flow in the presence of magnetic dipole, *Tech. Mech.,* **39** (2019), 3–15. https://doi.org/10.24874/ti.2019.41.03.12
19. I. A. Abdallah, Analytic solution of heat and mass transfer over a permeable stretching plate affected by chemical reaction, internal heating, Dufour-Soret effect and Hall effect, *Therm. Sci.,* **13** (2009), 183–197. https://doi.org/10.2298/TSCI0902183A
20. A. Zeeshan, A. Majeed, R. Ellahi, Effect of magnetic dipole on viscous ferrofluid past a stretching surface with thermal radiation, *J. Mol. Liq.,* **215** (2016), 549–554. https://doi.org/10.1016/j.molliq.2015.12.110

21. M. Nawaz, A. Zeeshan, R. Ellahi, S. Abbasbandy, S. Rashidi, Joules and Newtonian heating effects on stagnation point flow over a stretching surface by means of genetic algorithm and Nelder-Mead method, *Int. J. Numer. Method. H.,* **25** (2015), 665–684. https://doi.org/10.1108/HFF-04-2014-0103
22. K. Saeed, M. Shaban, S. Abbasbandy, Improved analytical solutions to a stagnation-point flow past a porous stretching sheet with heat generation, *J. Franklin I.,* **348** (2011), 2044–2058. https://doi.org/10.1016/j.jfranklin.2011.05.020
23. T. Hayat, T. Javed, Z. Abbas, Slip flow and heat transfer of a second-grade fluid past a stretching sheet through a porous space, *Int. J. Heat Mass Tran.,* **51** (2008), 4528–4534. https://doi.org/10.1016/j.ijheatmasstransfer.2007.12.022
24. J. M. Martin, I. D. Boyd, Momentum and heat transfer in a laminar boundary layer with slip flow, *J. Thermophysics Heat Tr.,* **20** (2006), 710–719. https://doi.org/10.2514/1.22968
25. M. E. Ali, The effect of variable viscosity on mixed convection heat transfer along a vertical moving surface, *Int. J. Therm. Sci.,* **45** (2006), 60–69. https://doi.org/10.1016/j.ijthermalsci.2005.04.006
26. Q. Li, Y. Xuan, Experimental investigation on heat transfer characteristics of magnetic fluid flow around a fine wire under the influence of an external magnetic field, *Exp. Therm. Fluid Sci.,* **33** (2009), 591–596. https://doi.org/10.1016/j.expthermflusci.2008.12.003
27. H. Yamaguchi, Z. Zhang, S. Shuchi, K. Shimada, Heat transfer characteristics of magnetic fluid in a partitioned rectangular box, *J. Magn. Magn. Mater.,* **252** (2002), 203–205. https://doi.org/10.1016/S0304-8853(02)00731-X
28. M. Motozawa, J. Chang, T. Sawada, Y. Kawaguchi, Effect of magnetic field on heat transfer in rectangular duct flow of a magnetic fluid, *Phys. Procedia,* **9** (2010) 190–193. https://doi.org/10.1016/j.phpro.2010.11.043
29. J. Bahram, S. Sadighi, P. Jalili, D. D. Ganji, Characteristics of ferrofluid flow over a stretching sheet with suction and injection, *Case Stud. Therm. Eng.,* **14** (2019), 100470. https://doi.org/10.1016/j.csite.2019.100470
30. Z. Ziabakhsh, G. Domairry, H. Bararnia, Analytical solution of non-Newtonian micropolar fluid flow with uniform suction/blowing and heat generation, *J. Taiwan Inst. Chem. E.,* **40** (2009), 443–451. https://doi.org/10.1016/j.jtice.2008.12.005
31. M. Ramzan, M. Farooq, T. Hayat, J. D. Chung, Radiative and Joule heating effects in the MHD flow of a micropolar fluid with partial slip and convective boundary condition, *J. Mol. Liq.,* **221** (2016), 394–400. https://doi.org/10.1016/j.molliq.2016.05.091

AIMS Press